Smart spiropyran-containing cellulose material for photopatterning, temperature and humidity sensing

Xue Zhou,[a] Jishuai Liu,[a] Congxia Xie,[a] Zhongtao Wu,[a] Lei Zhang,*[a] Xiliang Luo*[a]

[a]Key Laboratory of Optic-electric Sensing and Analytical Chemistry for Life Science, MOE; Shandong Key Laboratory of Biochemical Analysis; College of Chemistry and Molecular Engineering, Qingdao University of Science and Technology, Qingdao, 266042, China.
E-mail: zhanglei@qust.edu.cn, xiliangluo@qust.edu.cn

1. General remarks

Meterials: all starting materials, reagents and solvents for the synthesis of SPA were purchased and used without further purification. CMC was purchased from TCI. All the solutions were prepared using ultrapure water through a Millipore Milli-Q 185 water purification system (Millipore, USA).

Characterizations of SPA and CMC-SPA: ^{1}H NMR and ^{13}C NMR spectra were recorded on a Bruker Avance 500 (400 and 100 MHz, respectively) with $CDCl_3$ as a solvent. Chemical shifts were determined relative to the residual solvent peaks ($CHCl_3$, δ = 7.26 ppm for ^{1}H NMR, δ = 77.0 ppm for ^{13}C-NMR). The following abbreviations are used to indicate signal multiplicity: s, singlet; d, doublet; t, triplet; m, multiplet; br, broad. Mass spectra were recorded on a Thermo Scientific LTQ Orbitrap XL machine. TGA was carried out using a Netzsch STA 449C thermal analyzer in a nitrogen atmosphere and with a heating/cooling rate of 10 ^{o}C min^{-1}. DSC was performed by a Netzsch DSC204F1 machine with a heating rate of 5 ^{o}C min^{-1}. POM was conducted on a Nikon ECLIPSE LV100NPOL machine with a computational controlled heating plate. SAXS was performed by employing a conventional X-ray source with radiation wavelength of λ = 1.54 Å. The sample holder is a metal plate with a small hole (diameter ≈ 0. 5 cm, thickness ≈ 0. 5 cm), where the X-ray beam passes through and the sample-to-detector distance was 18 cm. The scattering vector q is defined as $q = 4\pi \sin\theta/\lambda$ with 2θ being the scattering angle. The UV-Vis absorption spectra were recorded on a Shimadzu UV-2600 UV-Vis spectrophotometer, and all the related studies were carried out on fast scan mode with slit widths of 1.0 nm, using matched quartz cells. Test solutions were 200 μL. The UV-Vis absorption spectra in solid state were measured by attaching thin test samples to the cell wall via a heating-cooling process. All absorption scans were saved as ACS II files and further processed in OriginLab software to produce all graphs shown. The wavelengths of UV and Vis photoirradiations are 365 nm (32 mW cm^{-2}) and 520 nm (96 mW cm^{-2}), respectively.

2. Synthesis and characterizations of SPA.

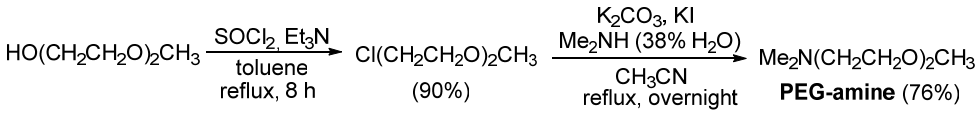

Scheme S1. Synthesis of PEG-amine.

2-(2-methoxyethoxy)-*N,N*-dimethylethan-1-amine (PEG-amine): PEG-amine was synthesized by following the reported procedures.[1, 2]

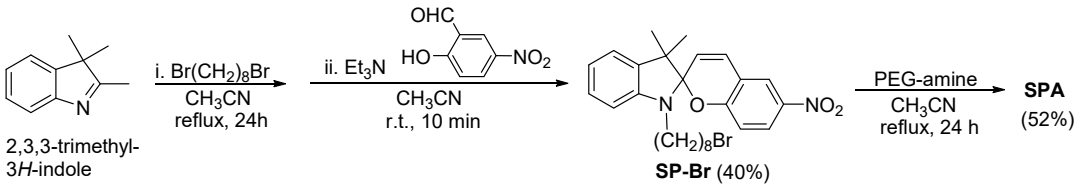

Scheme S2. Synthesis of SPA.

1'-(8''-Bromo-n-octyl)-3',3'-dimethyl-6-nitrospiro[2H-1-benzopyran-2,2'-indoline] (SP-Br): SP-Br was synthesized by following the reported procedures from us, and the ^{1}H NMR was in accordance with the reported data.[3, 4]

8-(3',3'-dimethyl-6-nitrospiro[chromene-2,2'-indolin]-1'-yl)-*N*-(2-(2-methoxyethoxy)ethyl)-*N,N*-dimethyloctan-1-aminium (SPA): to a solution of SP-Br (500 mg, 10 mmol) in acetonitrile (30 mL) was added PEG-amine (247 mg, 1.05 mmol, 1.05 eq) at r.t.. The resulting mixture was stirred over 24 h under reflux. After cooling to r.t., the mixture was concentrated *in vacuo*. The residue was purified by column chromatography on silica gel (DCM/MeOH = 10 : 1) to afford SPA/MCA (382 mg, 52% yield) as a solid. ^{1}H NMR (400 MHz, $CDCl_3$) δ 8.01-7.99 (m, 2 H), 7.17 (t, J = 7.2 Hz, 1 H), 7.08 (d, J = 6.8 Hz, 1 H), 6.94 (d, J = 10.4 Hz, 1 H), 6.85 (t, J = 7.2 Hz, 1 H), 6.74 (d, J = 9.6 Hz, 1 H), 6.55 (d, J = 8.0 Hz, 1 H), 5.86 (d, J = 10.4 Hz, 1 H), 4.02-3.94 (m, 2 H), 3.93-3.87 (m, 2 H), 3.67-3.65 (m, 2 H), 3.60-3.55 (m, 2 H), 3.52-3.50 (m, 2 H), 3.37 (s, 6 H), 3.34 (s, 3 H), 3.20-3.08 (m, 2 H), 1.65-1.58 (m, 2 H), 1.56-1.46 (m, 2 H), 1.33-1.22 (m, 8 H), 1.25 (s, 3 H), 1.18 (s, 3 H); ^{13}C NMR (125MHz, $CDCl_3$) δ 158.7, 146.0, 139.8, 134.9, 127.2, 126.7, 124.8, 121.7, 121.0, 120.7, 118.3, 117.6, 114.6, 105.7, 105.6, 70.6, 69.4, 64.9, 64.0, 62.2, 57.9, 51.6, 51.0, 43.0, 28.2, 27.8, 26.1, 25.2, 25.1, 21.9, 18.8; HRMS (ESI) calcd. for $C_{33}H_{48}N_3O_5^+$ 566.3588, found 566.3596.

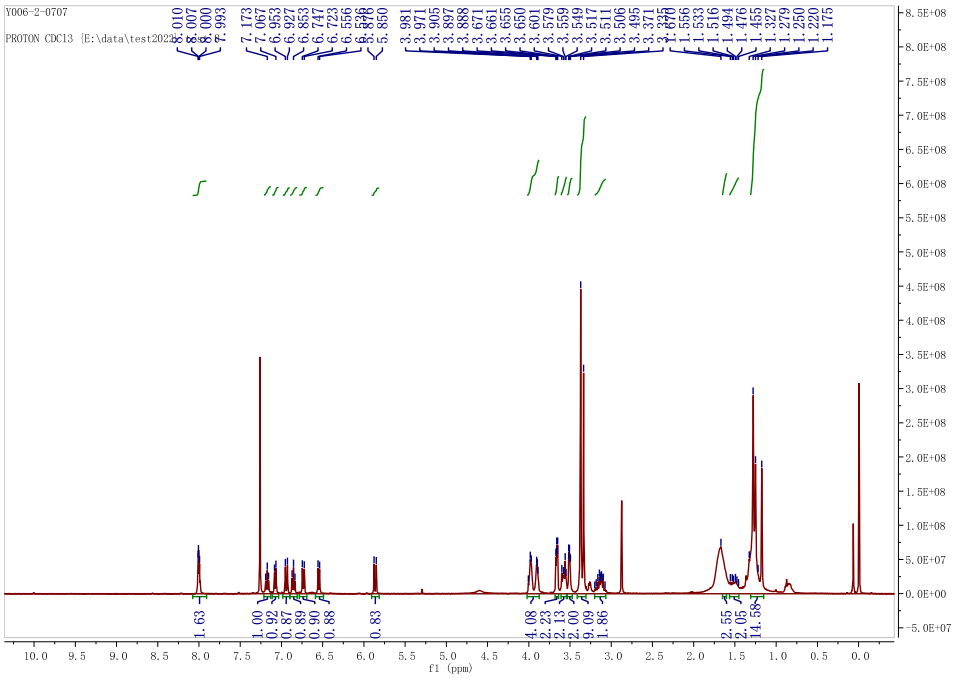

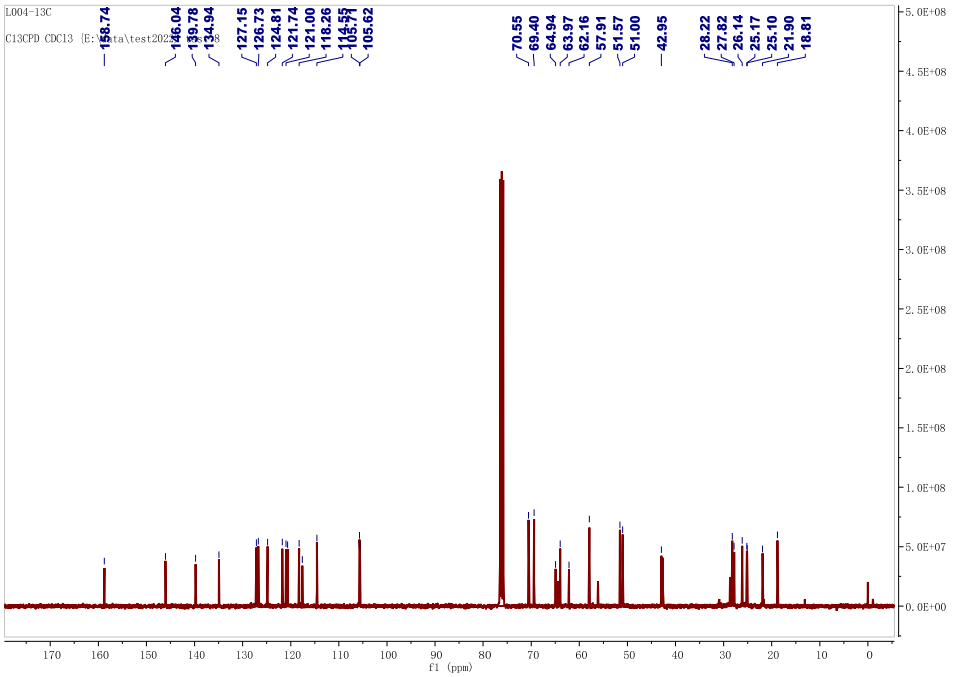

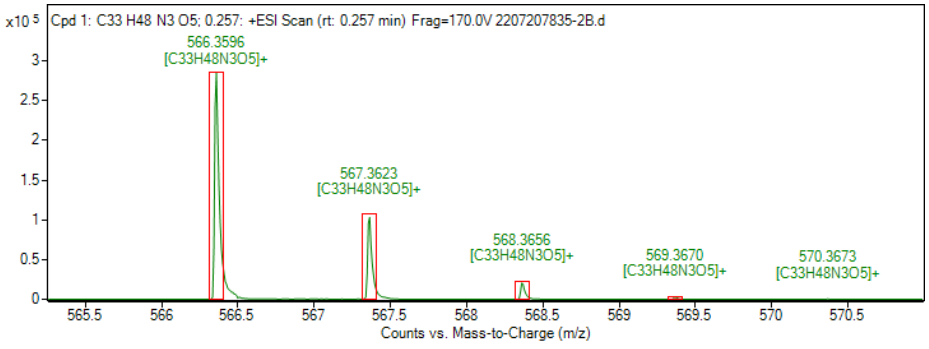

Figure S1. ^{1}H NMR, ^{13}C NMR and HRMS of SPA.

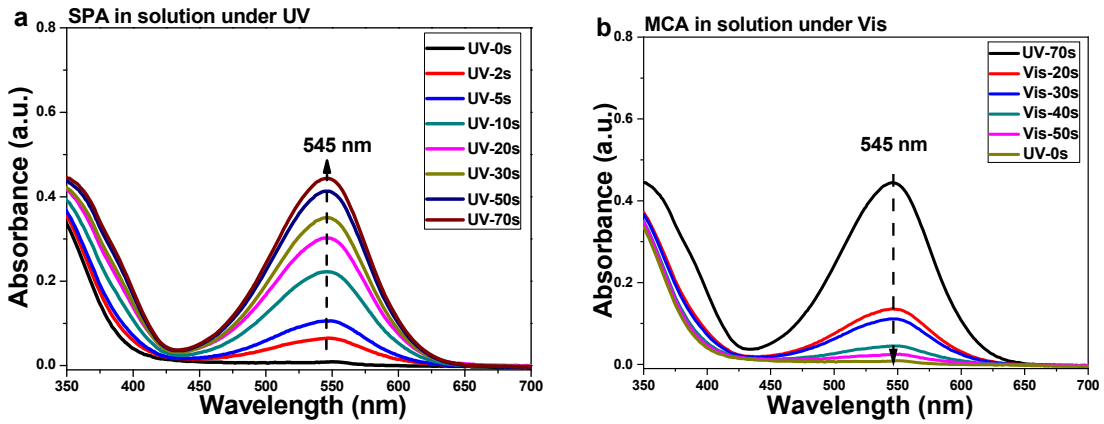

Figure S2. UV-Vis absorption changes of a) SPA under UV and b) MCA under Vis light in ethanol solution (50 μM) at r.t..

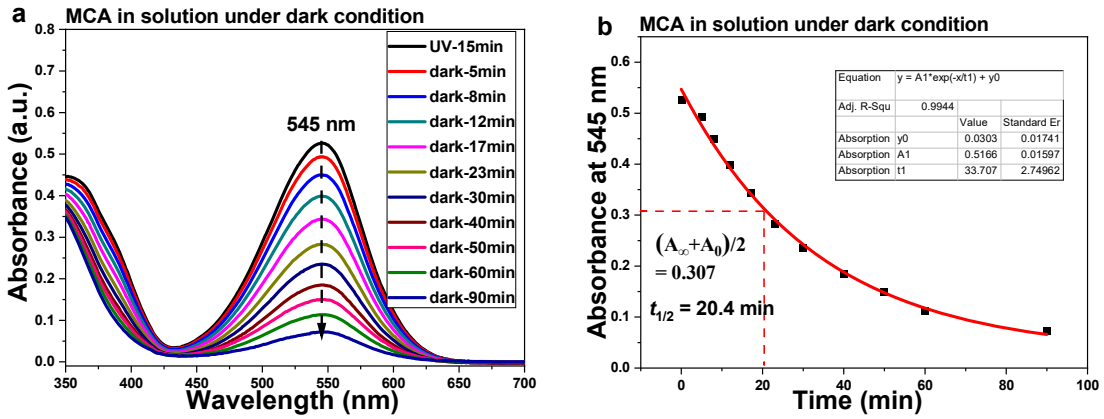

Equation of $\ln[(A_\infty-A_t)/(A_\infty-A_0)] = -\kappa_{rev}t$ is used for obtaining the thermodynamic MCA-to-SPA isomerization rate in dark, affording κ_{rev} = 0.089 min^{-1}, and $t_{1/2} = \ln2/\kappa_{rev}$ is used for obtaining the half-life of MCA in solution (Figure 2d), affording $t_{1/2}$ = ln2/0.089 = 7.8 min. A_∞ is the absorption intensity of MCA rich state after UV light irradiation. A_t is the absorption intensity of MCA at "t" time. A_0 is the absorption intensity of SPA rich state after isomerization.

Figure S3. Temporal evolved UV-Vis absorption spectral changes of MCA in ethanol solution (50 μM) at r.t. in dark. The π-π^* absorption intensity at 545 nm ie used for drawing the plotted graph.

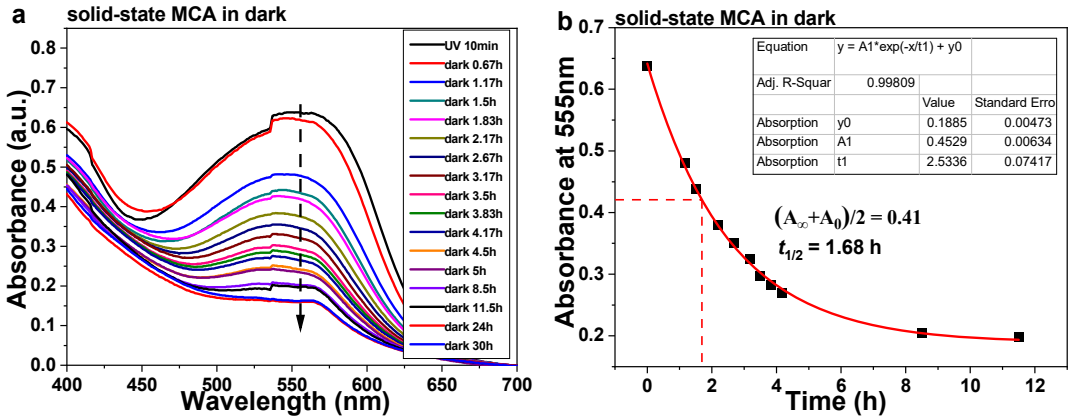

Similar as that in solution, with equations of $\ln[(A_\infty-A_t)/(A_\infty-A_0)] = -\kappa_{rev}t$ and $t_{1/2} = \ln2/\kappa_{rev}$, the half-life (1.61 h) of MCA in solid state could be obtained.

Figure S4. The temporal evolved UV-Vis absorption spectral changes of solid-state MCA in dark condition at r.t..

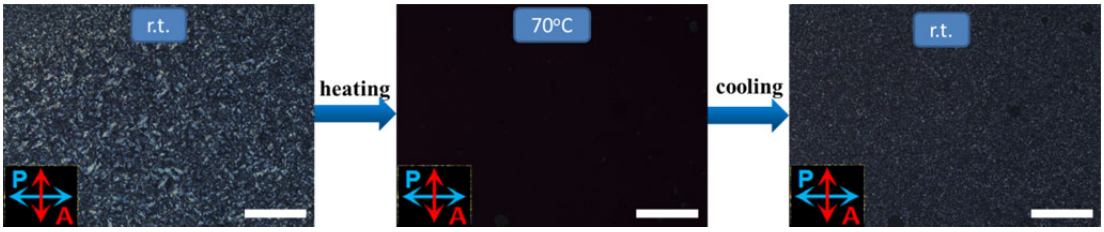

Figure S5. Temperature-dependent POM analysis of SPA. Scale bar: 100 μm.

3. Synthesis of CMC-SPA

Based on an assumption that one monosaccharide unit contains one negative charge, the aqueous solution of CMC-Na was prepared. The aqueous solution of SPA (30 mM, 400 μL) was added into the aqueous solution of CMC-Na (30mM, 600 μL) using a pipette. The precipitate was collected by centrifugation with rcf of 6124 g in an H1-16KR Centrifuge from Hunan Kechengyiqi Co., Ltd, China. The obtained precipitate was washed with water and centrifuged over three times. The resulted wet precipitate was pretreated with liquid nitrogen and then put into a SCIENTZ-10N Lyophilizer from Ningbo Scientz Biotechnology Co., Ltd, China for a lyophilization with -80^{o}C overnight, affording the needed CMC-SPA complexes.

4. Characterizations of CMC-SPA

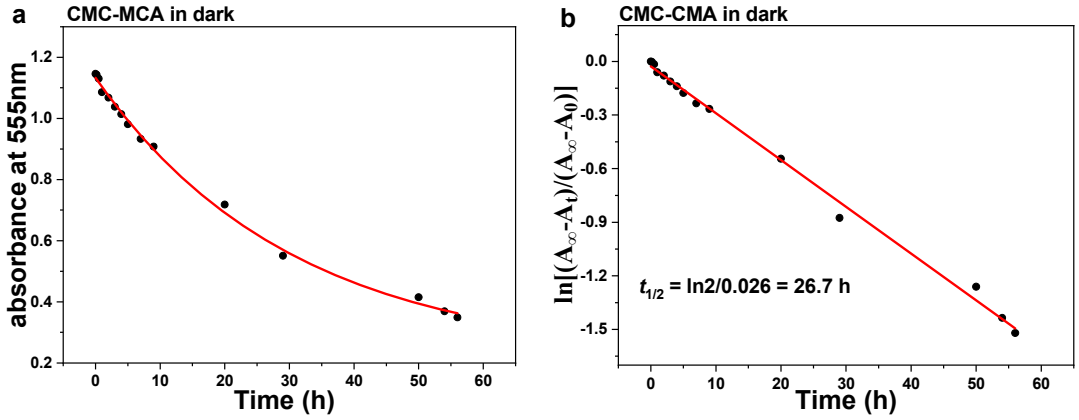

Similar as that in solution, with equations of $\ln[(A_\infty-A_t)/(A_\infty-A_0)] = -\kappa_{rev}t$ and $t_{1/2} = \ln2/\kappa_{rev}$, the half-life (26.7 h) of CMC-MCA in solid state could be obtained.

Figure S6. a) The plotted chart of absorbance change at 555 nm of CMC-MCA from Figure 3g. b) The calculation of half-life of MCA in ionic complex CMC-MCA.

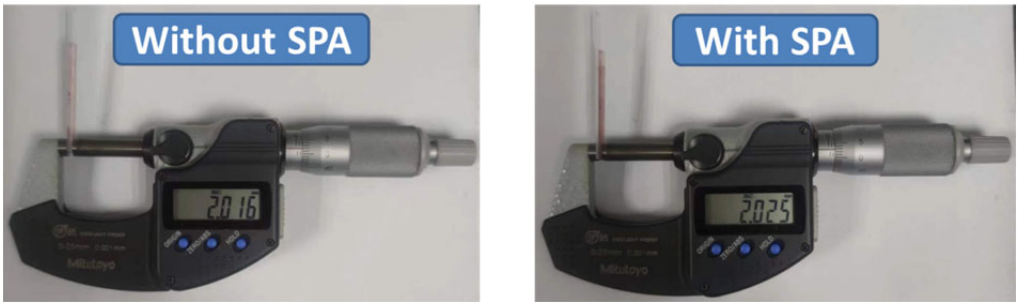

Figure S7. The thickness of SPA flake is determined as ca. 9 μm.

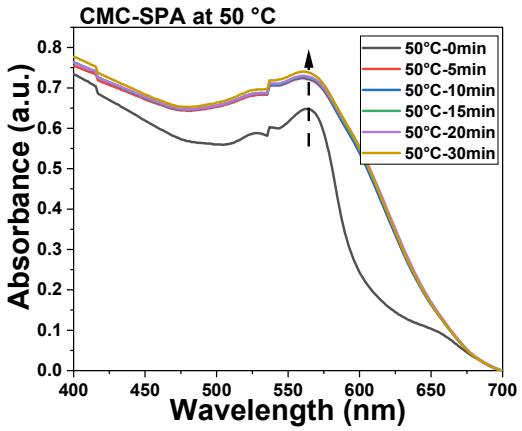

Figure S8. Temporal evolved UV-Vis absorption changes of CMC-SPA at 50 °C.

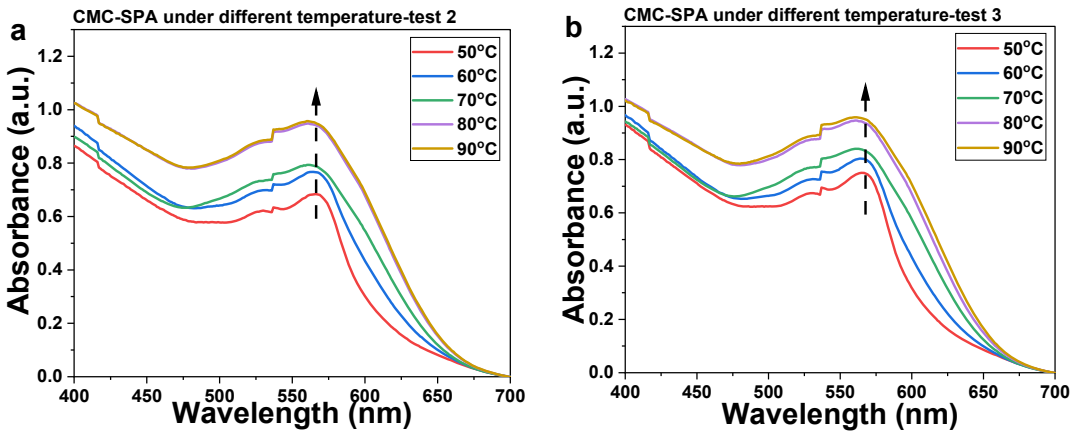

Figure S9. Temperature-dependent UV-Vis absorption changes of CMC-SPA were recorded in two more repeating groups.

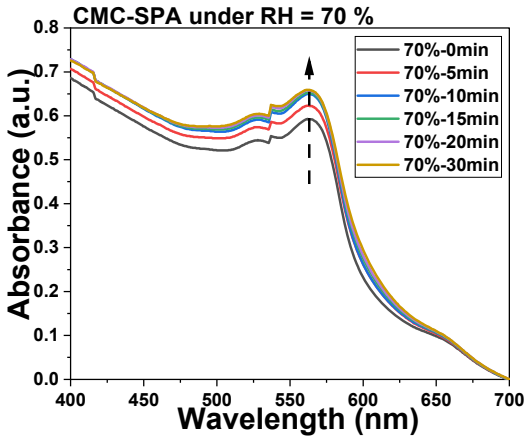

Figure S10. Temporal evolved UV-Vis absorption changes of CMC-SPA at r.t. under RH = 70%.

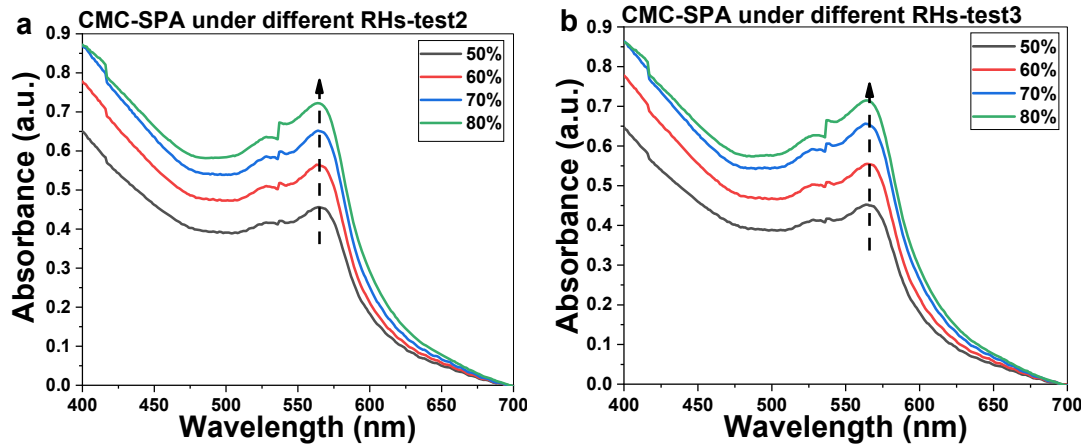

Figure S11. Humidity-dependent UV-Vis absorption changes of CMC-SPA at r.t. were recorded in two more repeating groups.

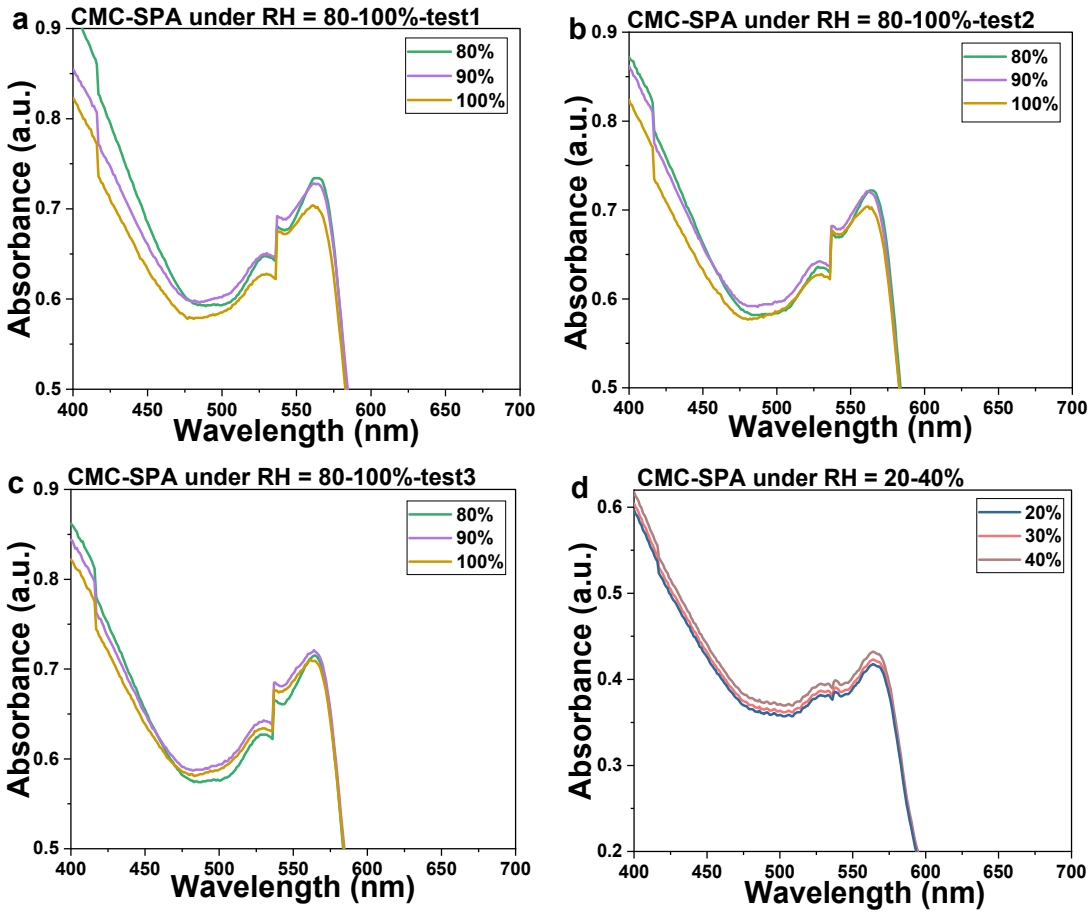

Figure S12. UV-Vis absorption changes of CMC-SPA under a-c) 80~100% and d) 20~40% at r.t..

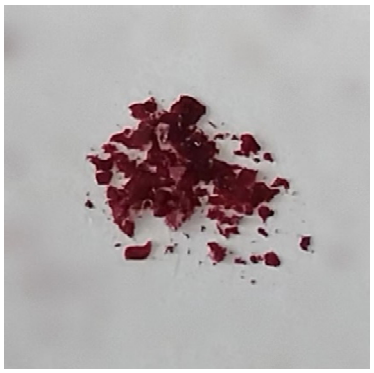

Figure S13. Image of CMC-SPATM.

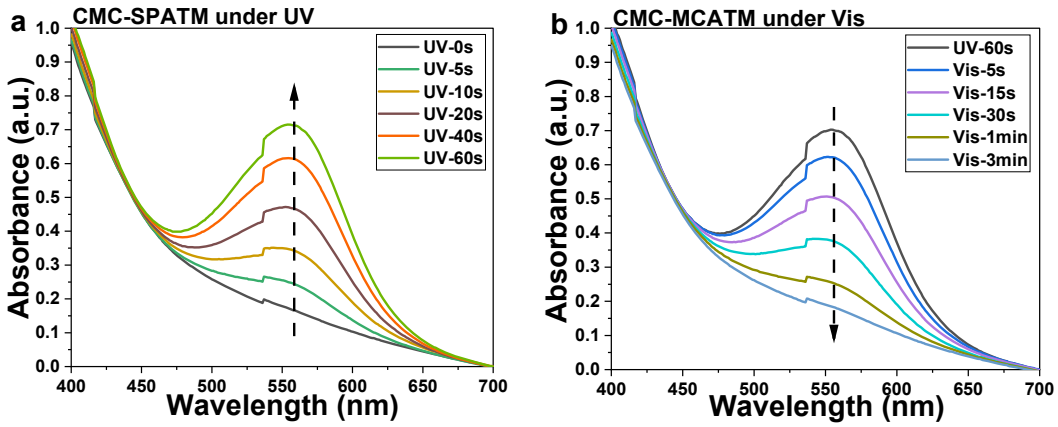

Figure S14. UV-Vis absorption changes of a) CMC-SPATM under UV light and b) CMC-MCATM under Vis light at r.t..

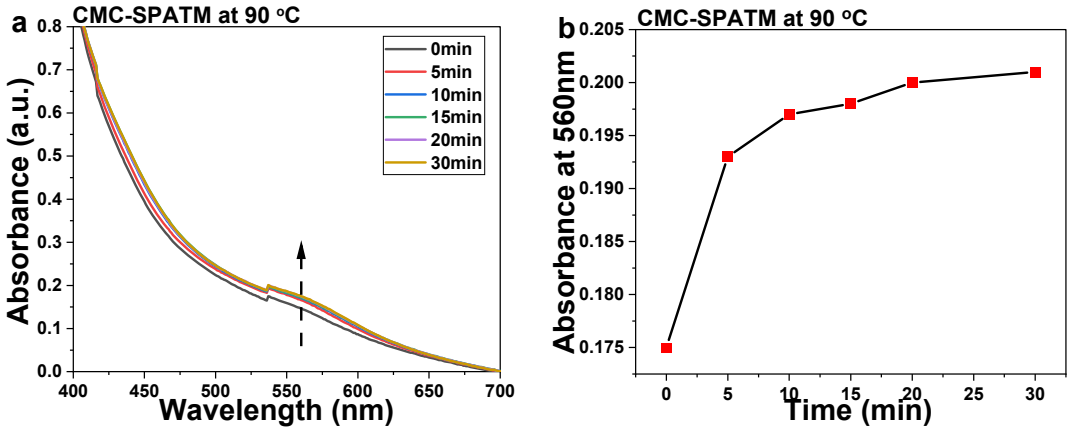

Figure S15. a) Temporal evolved UV-Vis absorption changes of CMC-SPATM at 90 °C. b) Plotted chart of UV-Vis absorption changes at 560 nm of CMC-SPATM at 90 °C, indicating that CMC-SPATM requires 10 min incubation for reaching a stable state.

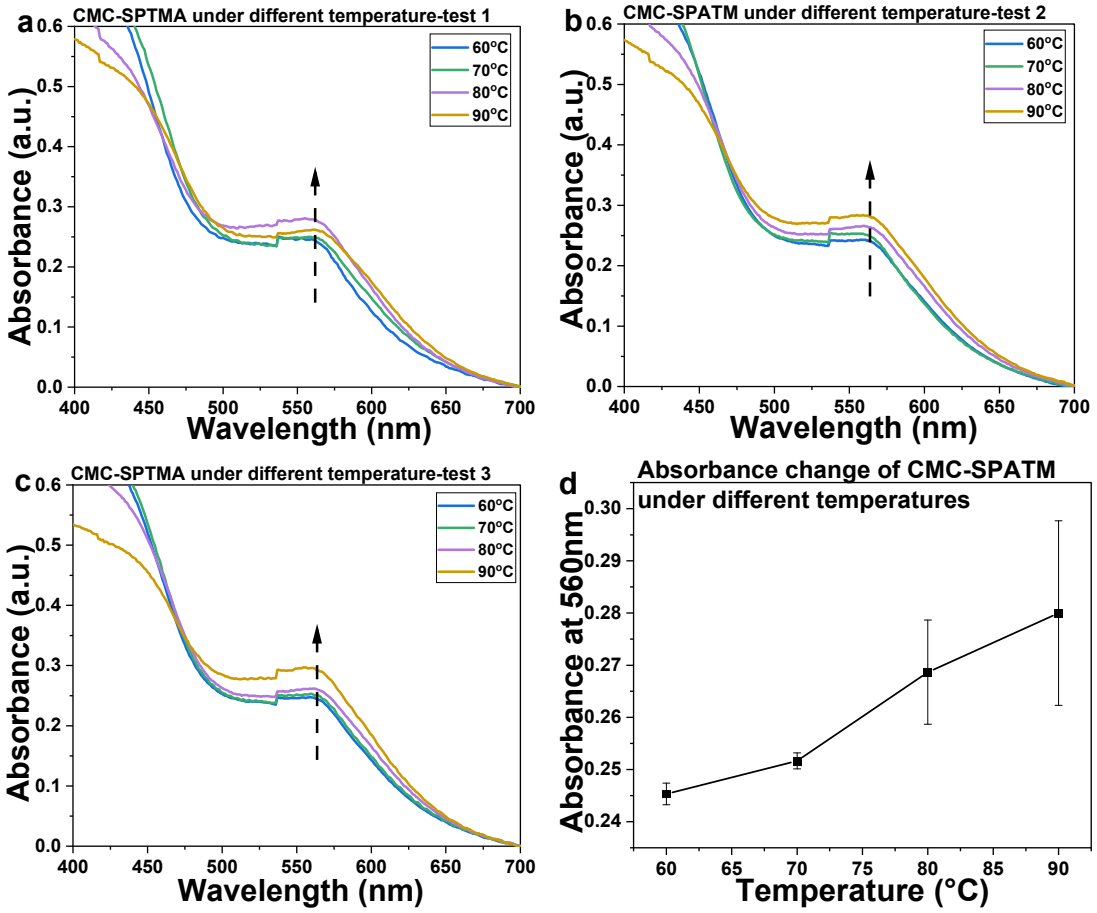

Figure S16. a-c) Temperature-dependent UV-Vis absorption changes of CMC-SPATM. d) Plotted chart of absorption change at 560 nm of CMC-SPATM at different temperatures, giving no linear relationship between absorbance and temperature.

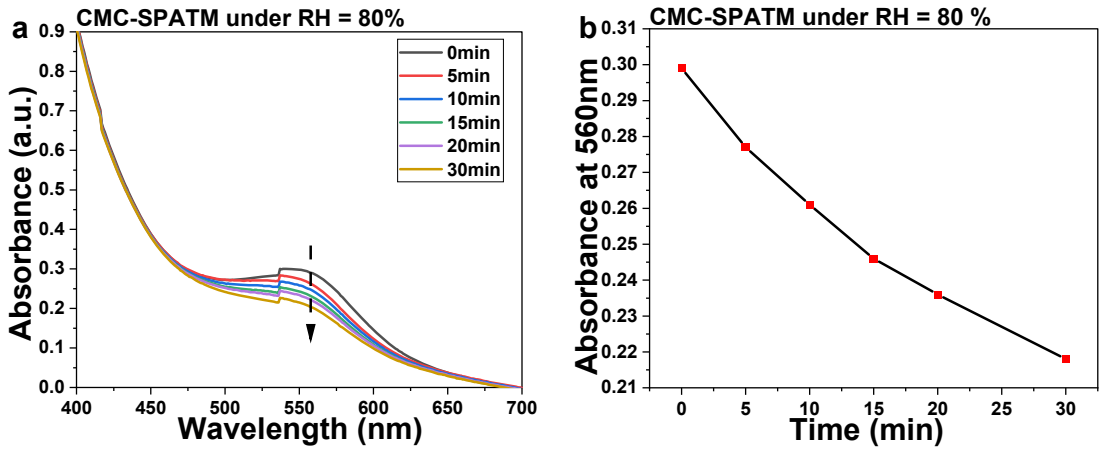

Figure S17. a) Temporal evolved UV-Vis absorption changes of CMC-SPATM at r.t. under RH = 80% within 30 min. b) Plotted chart of absorption change at 560 nm of CMC-SPATM under 80% RH, presenting a continuous decreasing trend of absorbance.

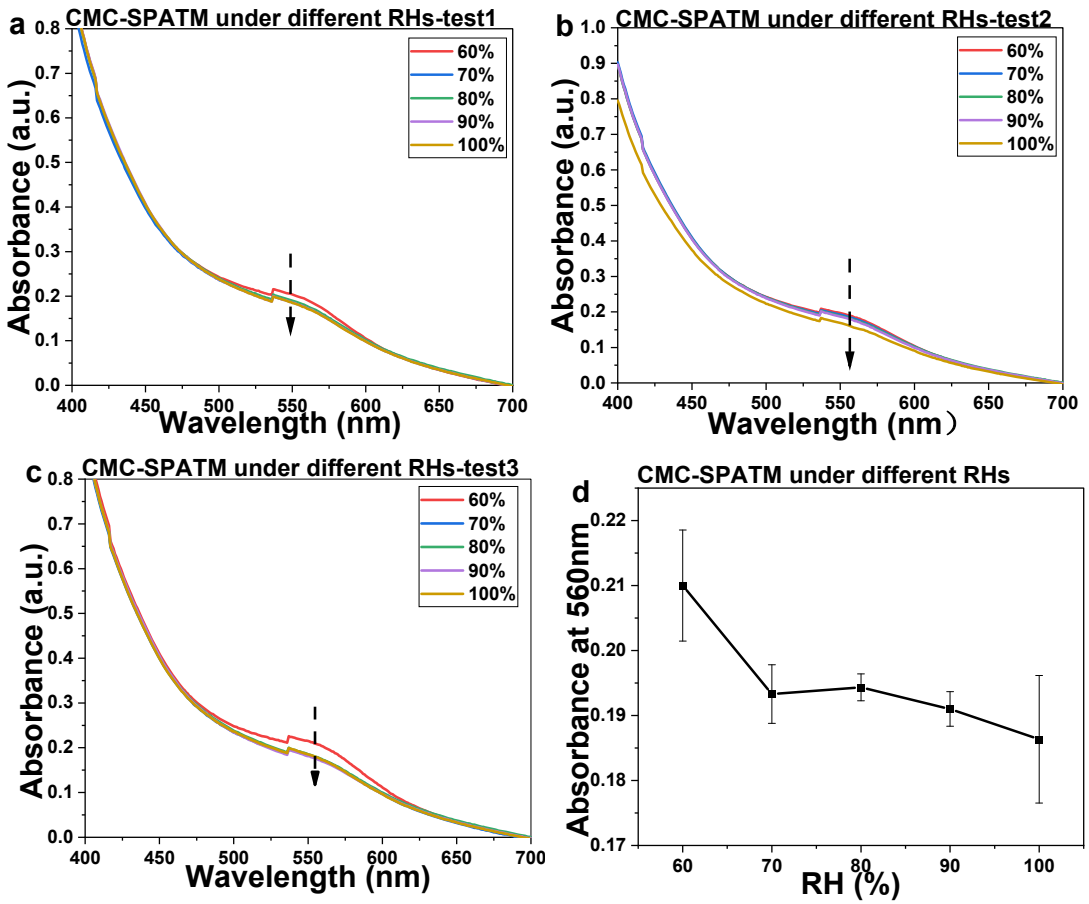

Figure S18. a-c) Humidity-dependent UV-Vis absorption changes of CMC-SPATM at r.t.. d) Plotted charts of absorption change at 560 nm of CMC-SPATM under different RHs.

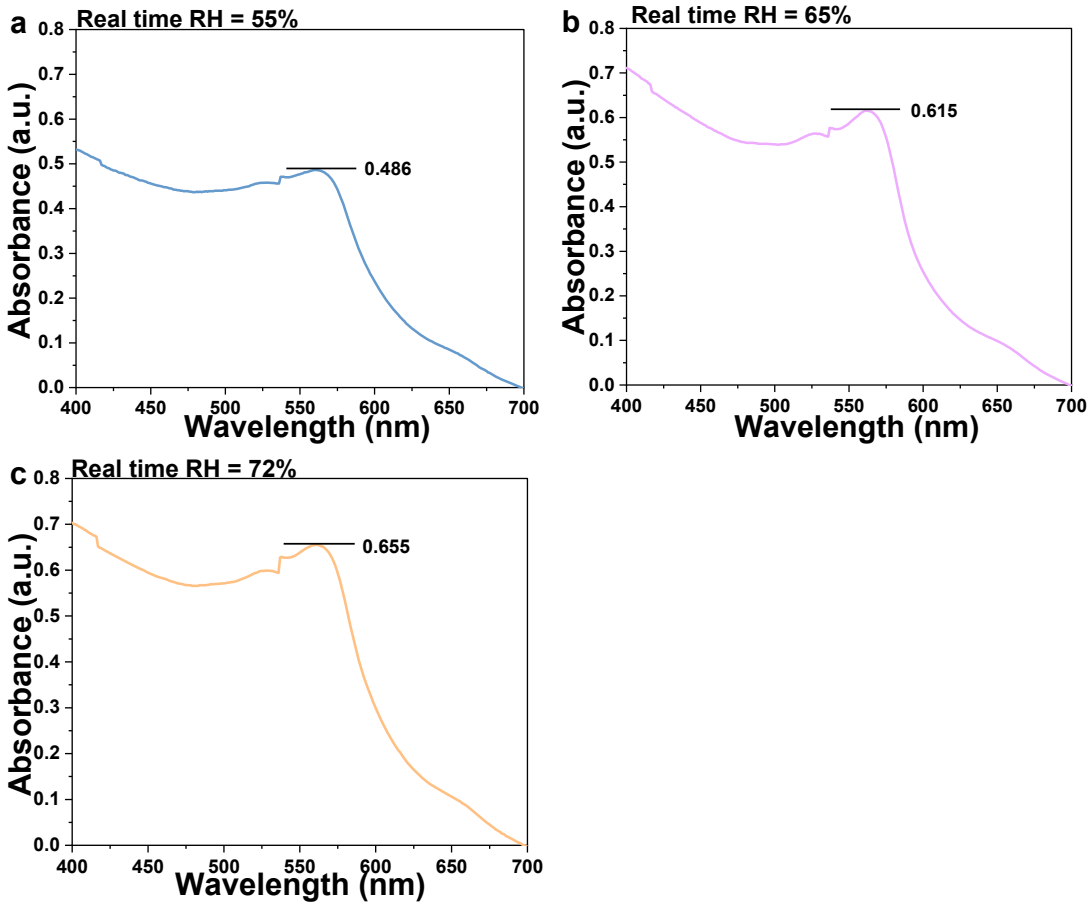

Figure S19. UV-Vis absorptions of CMC-SPA at r.t. under RH = a) 55%, b) 65% and c) 72% for 10 min.

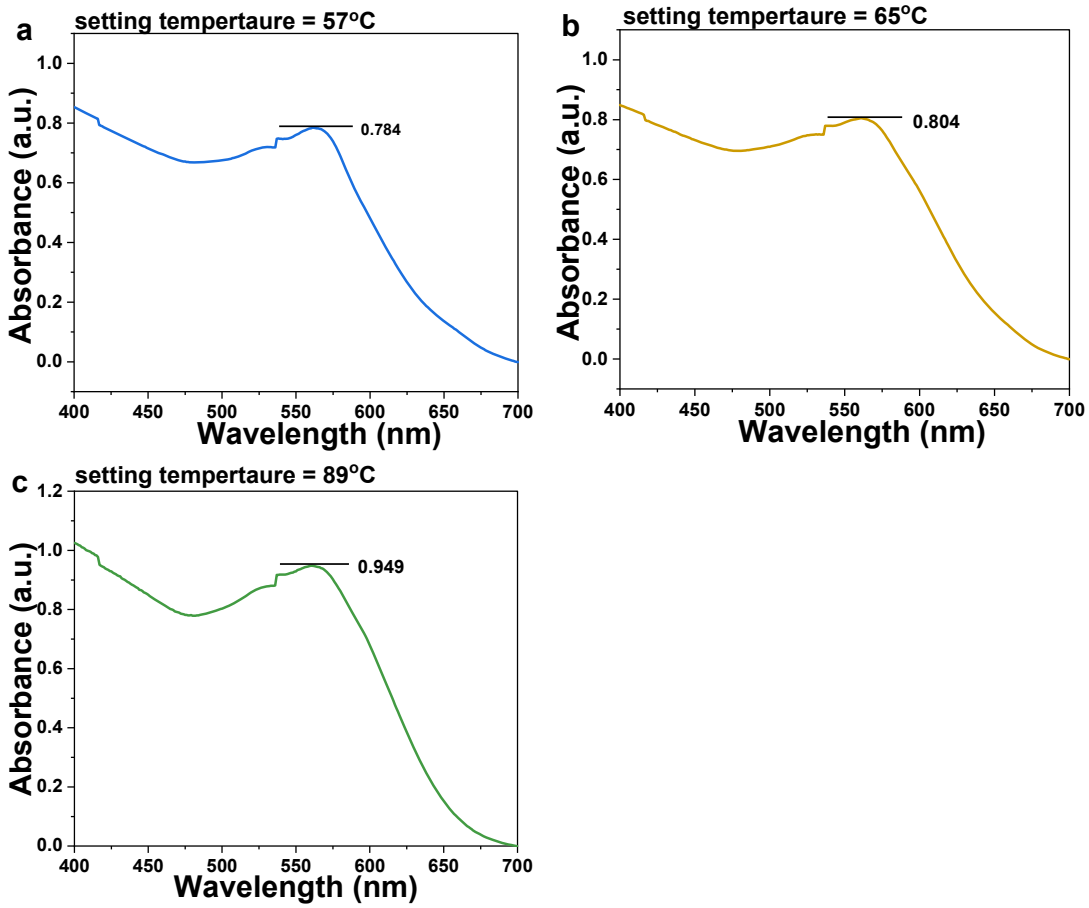

Figure S20. UV-Vis absorption of CMC-SPA in an oven with setting temperatures at a) 57 ^{o}C, b) 65 ^{o}C and c) 89 ^{o}C, respectively.

References

1. L. Zhang, Z. Tang, L. Hou, Y. Qu, Y. Deng, C. Zhang, C. Xie and Z. Wu, Selective mercury(ii) detection in aqueous solutions upon the absorption changes corresponding to the transition moments polarized along the short axis of an azobenzene chemosensor, *Analyst*, 2020, **145**, 1641-1645.
2. F. M. Ferrero Vallana, L. A. M. Holland, K. R. Seddon and O. Todini, Delayed release of a fragrance from novel ionic liquids, *New J. Chem.*, 2017, **41**, 1037-1045.
3. L. Zhang, Y. Deng, Z. Tang, N. Zheng, C. Zhang, C. Xie and Z. Wu, One-Pot Synthesis of Spiropyrans, *Asian J. Org. Chem.*, 2019, **8**, 1866-1869.
4. L. Zhang, Y. Deng, Y. Tang, C. Xie and Z. Wu, Solid-state spiropyrans exhibiting photochromic properties based on molecular flexibility, *Mater. Chem. Front.*, 2021, **5**, 3119-3124.